Available online at www.sciencedirect.com

SCIENCE DIRECT®

Nuclear Medicine and Biology 33 (2006) 193–202

NUCLEAR MEDICINE — AND — BIOLOGY

www.elsevier.com/locate/nucmedbio

Brain SPECT imaging and whole-body biodistribution with [^{123}I]ADAM—a serotonin transporter radiotracer in healthy human subjects

Kun-Ju Lin[a,b,c], Chia-Yih Liu[d,e], Shiaw-Pyng Wey[b,f], Ing-Tsung Hsiao[b,f], Jay Wu[g], Ying-Kai Fu[h], Tzu-Chen Yen[b,c,*]

[a]*Graduate Institute of Clinical Medical Sciences, Chang-Gung University, Tao-Yuan 333, Taiwan*
[b]*Molecular Imaging Center, Chang-Gung Memorial Hospital, Tao-Yuan 333, Taiwan*
[c]*Department of Nuclear Medicine, Chang-Gung Memorial Hospital, Tao-Yuan 333, Taiwan*
[d]*Neuroscience Research Center, Chang-Gung Memorial Hospital, Tao-Yuan 333, Taiwan*
[e]*Department of Psychiatry, Chang-Gung Memorial Hospital, Tao-Yuan 333, Taiwan*
[f]*Department of Medical Imaging and Radiological Sciences, Chang-Gung University, Tao-Yuan 333, Taiwan*
[g]*Health Physics Divisions, Atomic Energy Council, Institute of Nuclear Energy Research, Tao-Yuan 325, Taiwan*
[h]*Atomic Energy Council, Institute of Nuclear Energy Research, Tao-Yuan 325, Taiwan*

Received 8 July 2005; received in revised form 16 September 2005; accepted 12 October 2005

Abstract

Introduction: [^{123}I]-2-((2-((dimethylamino)methyl)phenyl)thio)-5-iodophenylamine ([^{123}I]ADAM), a novel radiotracer, has promising application in the imaging of the serotonin transporter (SERT) in the human brain. In this study, the optimal scanning time for acquiring brain single photon emission computed tomography (SPECT) images was determined by performing dynamic SPECT studies at intervals from 0 to 6 h postinjection of [^{123}I]ADAM. Additionally, radiation-absorbed doses were determined for three healthy human subjects using attenuation-corrected images.

Methods: Twelve subjects were randomized into one of three study groups as follows: whole-body distribution imaging ($n=3$), dynamic SPECT imaging ($n=3$) and brain SPECT imaging ($n=6$). The radiation-absorbed dose was calculated using MIRDOSE 3.0 software with attenuation-corrected data. The specific binding (SB) ratio of the brain stem was measured from dynamic SPECT images to determine the optimal scanning time.

Results: Dynamic SPECT images showed that the SB of the brain stem gradually increased to a maximum 4 h postinjection. Single photon emission computed tomography images at 4 h postinjection showed a high uptake of the radiotracer (SB) in the hypothalamus (1.40±0.12), brain stem (1.44±0.16), pons (1.13±0.14) and medial temporal lobe (0.59±0.10). The mean adult male value of effective dose was 3.37×10^{-2} mSv/MBq with a 4.8-h urine-voiding interval. Initial high uptake in SERT-rich sites was demonstrated in the lung and brain. A prominent washout of the radiotracer from the lung further increased brain radioactivity that reached a peak value of 5.03% of injected dose 40 min postinjection.

Conclusions: [^{123}I]ADAM is a promising radiotracer for SPECT imaging of SERT in humans with acceptable dosimetry and high uptake in SERT-rich regions. Brain SPECT images taken within 4 h following injection show optimal levels of radiotracer uptake in known SERT sites. However, dynamic changes in lung SERT distribution must be carefully evaluated.

Keywords: [^{123}I]ADAM; Biodistribution; Serotonin transporter; SPECT; Depression

1. Introduction

Dysfunction of the serotonergic system is associated with various psychiatric and neurological disorders such as depression, obsessive–compulsive disorder, schizophrenia, Alzheimer's disease and eating disorders [1–6]. The

* Corresponding author. Department of Nuclear Medicine, Chang-Gung Memorial Hospital, Tao-Yuan, Taiwan. Tel.: +886 3 3281200x2673; fax: +886 3 3280267.
E-mail address: yen1110@adm.cgmh.org.tw (T.-C. Yen).

0969-8051/$ – see front matter © 2006 Elsevier Inc. All rights reserved.
doi:10.1016/j.nucmedbio.2005.10.006

serotonin transporter (SERT) plays an important role in modulating presynaptic serotonergic function [7]. An autoradiographical study of postmortem human brains showed a reduction in SERT binding in the dorsal raphe nucleus in comparison to healthy subjects [8,9]. Imaging of the SERT by single photon emission computed tomography (SPECT) or positron emission tomography (PET) provides information on the integrity of the serotonergic neurotransmission in vivo [10,11]. Therefore, the use of noninvasive imaging techniques such as SPECT and PET can be valuable for early disease detection or for monitoring the progression of the serotonin pathogenesis, which is encountered in many of the aforementioned psychiatric and neurological disorders [9].

The development of radiopharmaceuticals, such as SPECT ligands, that are suitable for SERT imaging has been successful [12,13]. In particular, [^{123}I]beta-CIT demonstrated substantial uptake in the thalamus, hypothalamus and midbrain [14]. The addition of the selective serotonin reuptake inhibitor citalopram causes the displacement of [^{123}I]beta-CIT, thereby verifying that [^{123}I]beta-CIT selectively binds to SERT-rich sites [10,15]. However, small concentrations of SERT in the bilateral striatal regions create the potential for [^{123}I]beta-CIT binding with dopamine transporters (DATs) [15], further complicating the ability to clearly distinguish regions of SERT from DAT in [^{123}I]beta-CIT SPECT images.

[^{123}I]-2-((2-((dimethylamino)methyl)phenyl)thio)-5-iodophenylamine ([^{123}I]ADAM) is a novel radiotracer for targeting SERT [16–18]. Animal studies revealed this radiotracer to have properties superior to that of other radiopharmaceuticals, such as a high affinity and specificity for SERT [17,18]. In addition, quantitative and dynamic brain SPECT imaging has been investigated using nonhuman primates, which showed high uptake of [^{123}I]ADAM in the brain stem and hypothalamus regions [19,20]. To date, only preliminary human brain SPECT images have been published based on limited time points [21]. In these results, only the brain stem and hypothalamus SERT radioactivity can be identified, which differs from PET and autopsy results where SERT density can be demonstrated in the cortical areas. Our previous work indicated that individual brain regions with varying densities of SERT may have different transit equilibrium time periods after drug administration [17]. Single photon emission computed tomography image acquisition at different time periods might be helpful for distinguishing brain regions with varying SERT density.

Recently, two human biodistribution studies demonstrated reasonable uptake of [^{123}I]ADAM in the brain, lung and liver, suggesting [^{123}I]ADAM as a potential SERT radiotracer with acceptable dosimetry and high brain uptake [21,22]. However, a 50% difference in the effective dose equivalent (EDE) was reported in these two studies [21]. Because the bladder wall receives the largest proportion of the radiation dose after drug administration, a different approach for accurate urine radioactivity measurement might be helpful for accurate EDE estimation.

In this study, we determined the uptake of the [^{123}I]ADAM in brain regions using dynamic tomographic imaging. The dynamic protocol enabled correlation of the scanning time to the attainment of a maximum specific binding (SB) ratio in SERT-rich sites, which provided an accurate estimate of the optimal scanning time. We also evaluated the dosimetry with an in vitro counting method for an accurate measure of urine radioactivity and appropriate estimation of EDE.

2. Materials and methods

2.1. Radiopharmaceuticals

[^{123}I]ADAM with a high specific activity (>12 000 Ci/mmol) was prepared by an oxidative iododestannylation reaction modified from a previously described procedure [16]. Briefly, 100 μg of tin precursor, 2-((2-((dimethylamino)methyl)phenyl)thio)-5-(tri-*n*-butyltin)-phenylamine, was made to react with approximately 5.55 GBq (150 mCi) [^{123}I]NaI (INER, Lung-Tan, Taiwan) in the presence of hydrogen peroxide and diluted acetic acid for 5 min. After quenching with $NaHSO_3$, the neutralized reaction mixture was loaded on an octyl cartridge (Accubond, J&W Scientific, Folsom, CA, USA) for purification. The cartridge was washed with water and 50% ethanol to remove impure species. Purified [^{123}I]ADAM was obtained by eluting the cartridge with absolute ethanol. The purified [^{123}I]ADAM was then further diluted with 0.9% saline solution for the animal study. The radiochemical purity was determined by HPLC to be >90%.

2.2. Subjects

This study was approved by the Institutional Review Board of Chang-Gung Memorial Hospital. Twelve healthy subjects (five men and seven women) were included in the study (aged 30.8±6.7 years). Both the dynamic brain SPECT and the whole-body distribution studies included three subjects. The remaining six subjects received three brain SPECT images using the acquisition time determined in the dynamic brain SPECT study. All subjects were nonsmokers at the time of the study; 11 subjects had never smoked and 1 subject had not smoked for at least 2 years prior to study participation. Written informed consent was obtained from all subjects before study participation. The absence of medical, neurological and psychiatric abnormalities was verified by board-certified psychiatrists based on family history, physiological examination and routine blood tests. Other inclusion criteria were as follows: subjects aged between 20 and 40 years, absence of any previous psychotropic medication, no other *DSM-IV* axis I diagnosis, no history of alcohol or substance dependence or abuse, not pregnant during the study period, no concomitant or past severe medical conditions, no current suicidal or homicidal ideations and the ability to provide informed consent. All subjects, except one participant in the whole-body biodistribution

group who accidentally lost his drug, received Lugol's solution (containing 400 mg of potassium iodide) orally 2 days prior to the study in order to block thyroid uptake of dissociated [^{123}I].

2.3. Brain SPECT image acquisition

The healthy volunteers received a mean dose of 185± 4.1 MBq of [^{123}I]ADAM intravenously as a single bolus. After tracer injection, any possible adverse or subjective feelings related to the injection procedure was processed on a predefined adverse chart. Subjects were also requested to rate the tolerance of the tracer injection and the scanning protocol on a scale from 1 to 10, 10 being untolerable. Brain SPECT images were acquired with a Siemens E.CAM dual head gamma camera (Siemens Medical Systems, Hoffman Estates, IL) equipped with fan-bean collimators. The radius of rotation was 16.4 cm, and the focal length of the fan-bean collimators was 51 cm. The matrix size was 128×128 pixels. The energy window was set at 159 keV with a 20% symmetric window. Dynamic SPECT images were acquired with 60 projection angles per detector over 180° at a magnification of 1.23. Acquisition protocols for subjects 1 to 3 involved three phases of image collection. The first series of images was collected starting at 0 min postinjection and was stopped at 60 min postinjection. Each scan lasted 12 min and was repeated four times every 15 min. The second phase of image collection was initiated at 60 min and stopped at 4 h postinjection. The acquisition time was 24 min and the scans were repeated six times every 30 min. Finally, the third phase involved the collection of two 48-min scans at 5 and 6 h postinjection. After reviewing the images from subjects 1 to 3, a modified protocol entailing three 48-min scans at 3, 4 and 5 h postinjection was performed on subjects 4 to 9.

2.4. Magnetic resonance imaging

Magnetic resonance imaging (MRI) was conducted for each subject in order to provide a structural reference for the functional SPECT images. The structure–function correlation was accurately determined by coregistration of the MRI images to the SPECT images. Magnetic resonance imaging data were acquired on a VISION VB33D 1.5-T instrument (Siemens Medical Systems). T1-weighted axial images (repetition time [TR], 500 ms; echo time [TE], 25 ms) and T2-weighted axial images (TR, 3500 ms; TE, 120 ms) were obtained in the transaxial plane (0.781 mm thickness and 3 mm gap). Magnetic resonance imaging images were resized and resliced in planes parallel to the orbitomeatal line.

2.5. Whole-body image acquisition

Whole-body scans were performed using an Elscint VariCam dual-headed gamma camera equipped with a parallel-hole medium-energy collimator and a 20% symmetric energy window centered on a photopeak of 159 keV. All images were acquired with a constant scanning speed of 15 cm/min (scanning speed, 7.5 cm/min 24 h postinjection) into a 1024×256 matrix. A reference source of approximately 0.37 MBq was imaged with the subject in order to confirm a consistent set of serial planar images. A whole-body transmission scan was performed in subjects prior to the injection of [^{123}I]ADAM by placing a bar source containing 370 MBq of [^{123}I] at the posterior camera head and recording the image from the anterior head. Serial whole-body images were obtained at 5 and 40 min and 1.5, 2, 3, 4, 6 and 24 h after intravenous injection of 182±2.1 MBq [^{123}I]ADAM. All image acquisitions included the entire body for complete counting of whole-body activity. Urine was collected at specific postinjection intervals (0–6, 6–12, 12–18 and 18–24 h) in all three subjects. For each interval, three 1-ml urine aliquots from each subject were counted in a well counter (Perkin-Elmer Wallac, Model 1470 Wizard). The counting efficiency of the well counter was determined by a known calibrated [^{123}I] radioactivity source with the same geometry as the samples. The decay-corrected radioactivities were then multiplied by the urine volume in each sampling time interval. All urine radioactivities are expressed as percentage of injected dose (%ID).

2.6. Brain SPECT image analysis

The filtered backprojection algorithm was implemented in order to reconstruct the SPECT projection data using a Metz filter (cut-off, 0.30 cycles/pixel; order, 12) on a 128× 128 pixel matrix. Attenuation correction was performed by assuming uniform attenuation within an ellipse drawn around the head contour (attenuation coefficient, 0.12/cm). The slice thickness and pixel size were 3.895 mm. Initially, each subject's SPECT image was automatically coregistered with the corresponding MRI image. The two images were then manually aligned by visual inspection of the overlaid images using the multimodality software PMOD (PMOD Technologies, Zurich, Switzerland). Volumes of interest (VOIs) corresponding to the frontal cortex, striatum, thalamus, hypothalamus, medial temporal lobe, brain stem, pons and cerebellum were drawn on the coregistered image using the MRI image as the structural reference. No correction was made for partial volume effect because all VOIs were restricted to regions completely within the target to minimize this problem. All measured count densities were decay-corrected to the time point of tracer injection. For analysis, the cerebellum, assumed to be devoid of SERT, served as the reference region [23]. The SB of [^{123}I]ADAM in each brain region was calculated using the equation $[(VOI_{target}-VOI_{cerebellum})/VOI_{cerebellum}]$. Brain regional uptake was calculated as counts per minute per megabecquerel injected dose with radioactivity decay correction (counts per minute per pixel per megabecquerel).

2.7. Whole-body biodistribution

Biodistribution of [^{123}I]ADAM was quantified by serial whole-body planar scans after injection of the radiotracer. The image data were analyzed using Image Gauge version

3.46 (Fuji Photo Film, Japan). The consistency of the whole-body emission scans was validated by measuring the activity of a reference source at a fixed region of interest (ROI) at time points equal to the physical decay of [^{123}I]. Regions of interest were drawn on the earliest anterior image and placed abutting each other for the following organs: brain, thyroid, lungs, heart, liver, gallbladder, kidneys, small intestine, upper large intestine, lower large intestine and the remainder of the body. Shapes and sizes of ROIs were kept constant for all subsequent images. The same set of ROIs was placed on serial posterior images after horizontal flipping.

Attenuation correction was calculated as follows: transmission factors reflecting the fraction of counts passing through the ROIs were calculated in each subject as the ratio of the counts/pixel measured over each organ to the counts/pixel for an unattenuated off-body region. The same set of ROIs was then applied to the emission images. Correction for the attenuation of the conjugated count emission images was performed by dividing the geometric mean (the square root of the anterior and posterior counts in each ROI) by an attenuation correction factor equal to the square root of the transmission factor.

For biodistribution evaluation, the geometric mean of the measured counts in each target organ and remainder was calculated. Conjugated counts were corrected for regional attenuation as described above. Measurements were corrected for physical decay. The total amount of activity in each target organ and remainder was expressed as %ID, calculated by dividing the organ activity by the total amount of injected activity in the first whole-body scan (i.e., sum of attenuation-corrected activity in each organ and remainder) before a urine voiding.

For dosimetry evaluation, the attenuation-corrected geometric mean of the measured counts in each target organ and remainder was calculated. Time–activity curves of each source organ and remainder were plotted without decay correction. The area under the curve of each organ was calculated using the trapezoidal method. The area under the curve at 24 h was calculated by assuming that the decline in radioactivity after this time point was solely dependent on physical radioactivity decay. Calculating the area under the curve for the fraction of injected dose from time $t=0$ to infinity yields the residence time. For each subject, the urine activity was corrected for physical decay. The amount of radioactivity in the urine at each voidance was expressed as %ID of [^{123}I]ADAM. A monoexponential curve was fitted to the cumulative urine activity, and the total urine excretion as a fraction of the injected dose and the biological half-life were determined. Target organ radiation-absorbed dose, effective dose (ED) and EDE were calculated by applying the MIRD schema using the MIRDOSE 3.0 software package (Oak Ridge National Laboratories, Oak Ridge, TN, USA). Calculation of residence times of the urinary bladder wall at urine-voiding intervals of 2.4 and 4.8 h was performed using the dynamic bladder model. Radiation dose estimates were calculated for each individual subject using a reference phantom of an adult male (70 kg).

3. Results

There were no adverse or subjective effects in any of the patients after injection of 185 MBq [^{123}I]ADAM. The vital signs of the patients remained stable throughout the experiment, and there were no significant changes in clinical

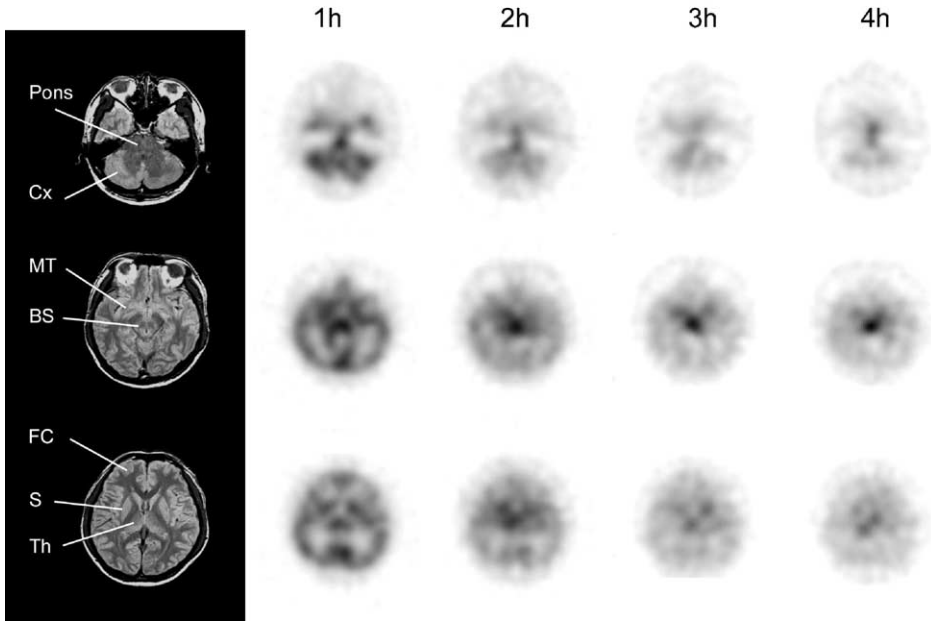

Fig. 1. A sequence of transverse slices of [^{123}I]ADAM SPECT images acquired 1 to 4 h posttracer injection and corresponding MRI scans. Various VOIs are defined as follows: Cx, cerebellum; Pons, pons; BS, brain stem; MT, medial temporal lobe; Th, thalamus; S, striatum; and FC, frontal cortex. Image intensities were normalized to their global maximum.

laboratory parameters before and 6 h after administration of the radiotracer.

3.1. Distribution of [^{123}I]ADAM in the brain

Following injection of the [^{123}I]ADAM tracer, accumulation was observed in regions known to have high concentrations of SERT including the brain stem, hypothalamus, medial temporal lobe and pons (Fig. 1). Fig. 2A shows the time–activity curve of various brain regions after tracer injection. Radioactivity in each brain region reached a peak approximately 45 min postinjection. High peak uptake values were seen in the brain stem and hypothalamus, followed by the pons, thalamus, striatum, medial temporal lobe and frontal cortex. The lowest uptake was noted in the cerebellum; thus, it was selected as a reference region for SB calculations. A set of SB curves for the various brain regions are shown in Fig. 2B. The SB of the brain stem and hypothalamus increased gradually over time and reached a peak value 4 h after radiotracer injection. The striatum, pons and thalamus attained a peak SB approximately 2 to 3 h postinjection. On reaching a maximum, the SB in all brain regions remained constant until 6 h postinjection.

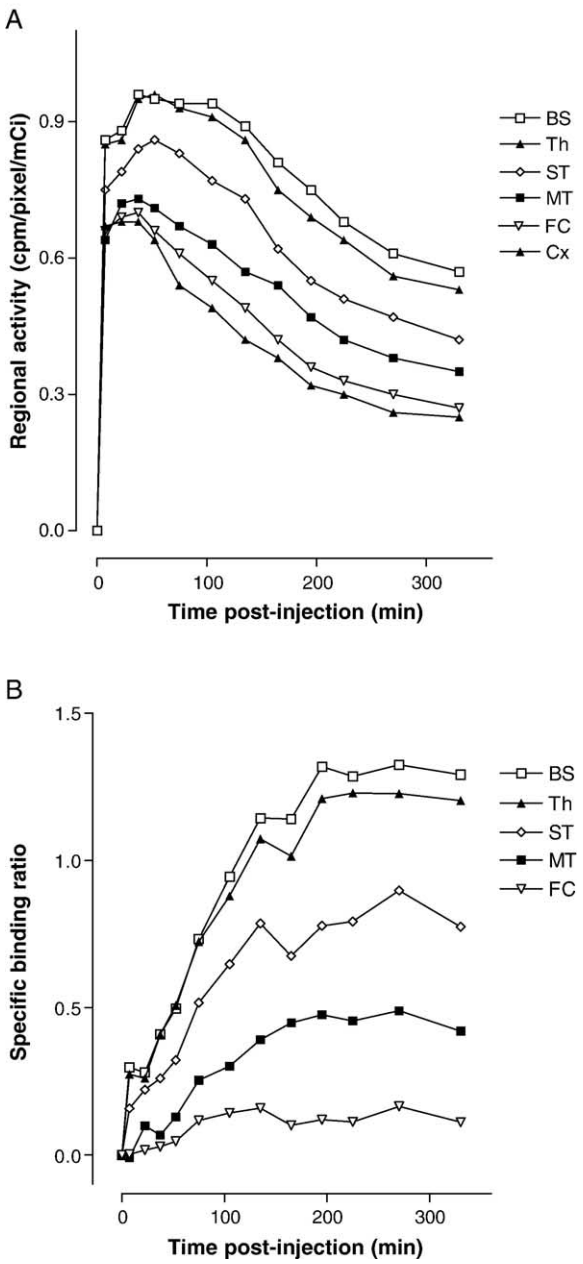

Fig. 2. Time–activity curves (A) and SB (B) of various brain regions measured from three dynamic SPECT studies.

Table 1
The mean SBs of the three study times for all VOIs (n=9)

Scanning time	3 h postinjection (%)		4 h postinjection (%)		5 h postinjection (%)	
	Mean	S.D.	Mean	S.D.	Mean	S.D.
Frontal cortex	0.16	51	0.14	55	0.15	77
Right striatum	0.79	15	0.80	20	0.81	23
Left striatum	0.80	14	0.81	19	0.83	21
Thalamus	1.04	14	1.10	13	1.12	16
Hypothalamus	1.21	9	1.40	8	1.39	6
Brain stem	1.19	11	1.44	11	1.42	8
Pons	0.97	11	1.13	12	1.12	16
Right medial temporal lobe	0.50	16	0.60	17	0.56	25
Left medial temporal lobe	0.48	17	0.59	17	0.56	25

According to the above dynamic SPECT results, all brain regions reached their transit equilibrium by 4 h. Therefore, three additional SPECT images were acquired between 3 and 5 h postinjection from six subjects for further evaluation. Table 1 shows SB values from the brain regions for nine subjects at three different time points postinjection. The SB of the brain stem reached a peak value of 1.44 at 4 h postinjection. At three different time points, no significant differences in SB values were evident between the groups. The SB of the hypothalamus, pons and medial temporal lobe 4 h postinjection were 1.40, 1.13 and 0.60, respectively.

The boundary of striatal radioactivity was difficult to identify solely by viewing the low-count dynamic SPECT images. However, fusing corresponding images obtained from SPECT and MRI can enhance the information provided exclusively by each modality. Correlating the functional information from SPECT with the anatomical information obtained from MRI enabled the boundary of the striatal radioactivity (the VOI) to be identified. The resulting SB value was calculated to be 0.81. There was no significant difference in SB values between the right and left striatum and medial temporal lobes.

3.2. Biodistribution

Whole-body images of [^{123}I]ADAM biodistribution at various intervals postinjection are shown in Fig. 3 for a single representative subject. The brain, lungs, liver, gallbladder, intestinal tract and bladder were visually identified on the whole-body emission images as organs with moderate to high activity. Five minutes after tracer

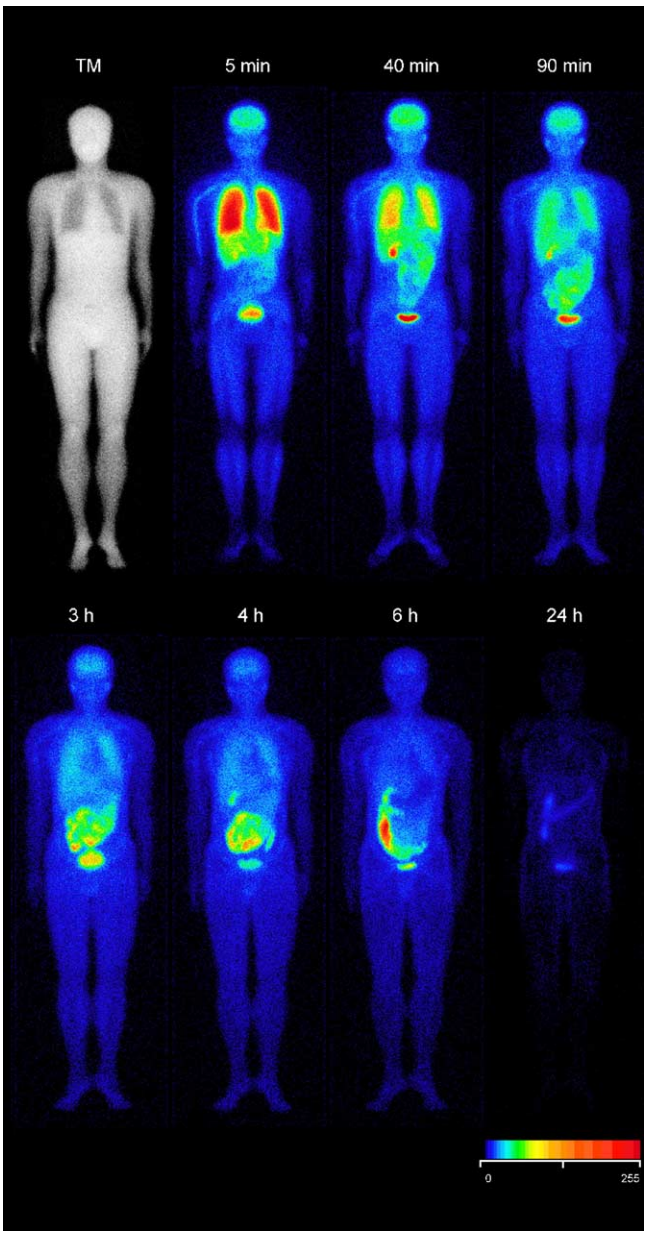

Fig. 3. Anterior whole-body transmission and emission images of a healthy volunteer taken at time intervals ranging from 5 min to 24 h postinjection of [^{123}I]ADAM. The intensity of the emission images acquired at different times after radiotracer injection was decay-corrected, normalized to the same acquisition speed and normalized to their global maximum for comparison. A rainbow color scale was applied to all of the emission images (TM: transmission scan).

injection, the highest peak values of %ID (decay corrected) were found in the lungs and liver (29.0 and 9.86 %ID, respectively). Forty minutes later, uptake in the lung decreased sharply to 16.2 %ID. Simultaneously, brain uptake reached an overall maximum value of 5.02 %ID. Peak uptake values were seen in the intestine at a lateral time between 120 and 240 min after tracer injection, as shown in Fig. 4A and B. Although the kidneys did not demonstrate substantial uptake, the accumulated radioactivity in the urine was 32.6 %ID in the first 6 h of collection, suggesting considerable excretion of the radioactivity through the renal system. Fig. 5 shows the dynamic accumulation of radioactivity in the urine for the three subjects. A monoexponential curve was fitted to the accumulated urine radioactivity data with a R^2 value of 0.94±0.02. The average (mean±S.D.) biological half-life was 2.34±0.17 h, and the average total accumulation of urine radioactivity was 52.9±8.8 %ID, determined by fitting a monoexponential curve to infinite time. Urinary bladder content residence times of 0.59±0.09 and 1.24±0.18 h for 2.4- and 4.8-h urine-voiding intervals, respectively, were determined using the dynamic bladder model.

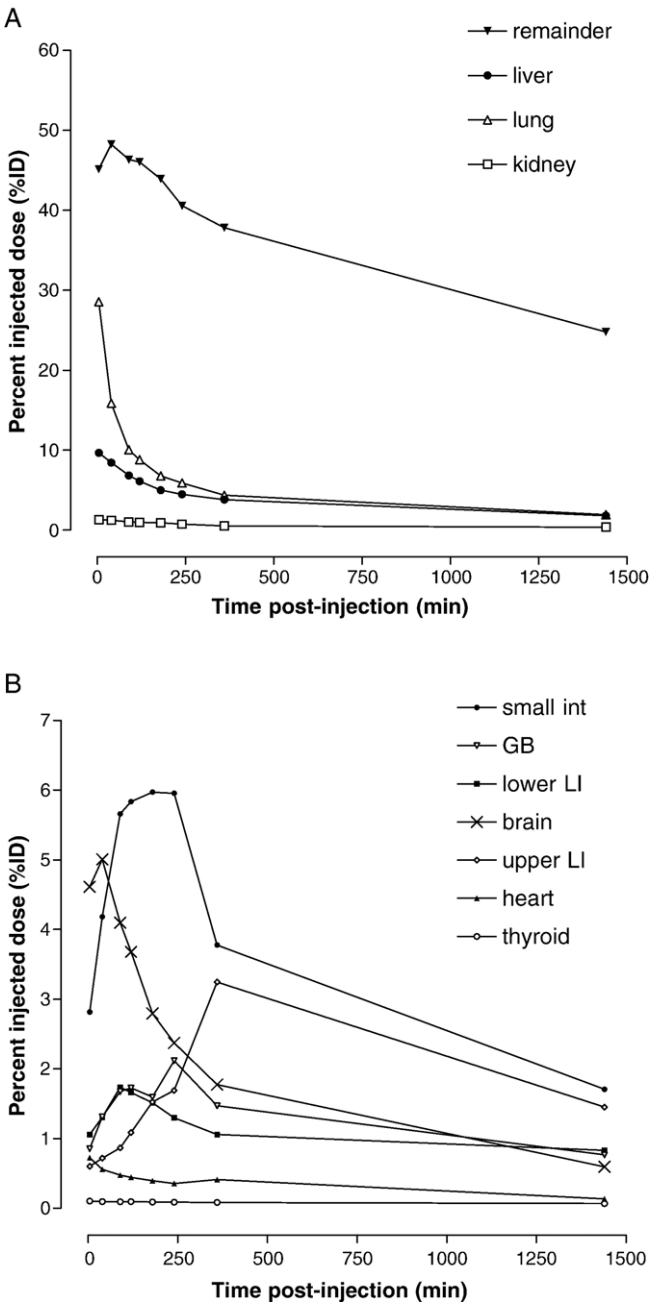

Fig. 4. Whole-body distribution of [^{123}I]ADAM in three healthy subjects with decay correction.

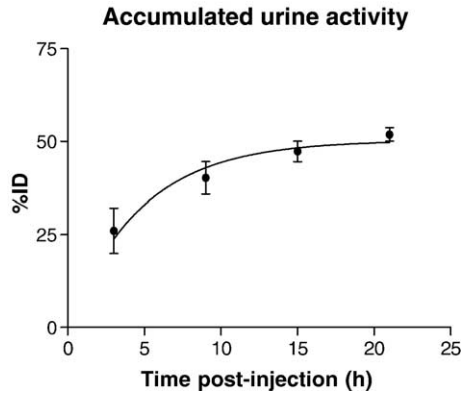

Fig. 5. Cumulative decay-corrected activity in urine following intravenous administration of [^{123}I]ADAM in three healthy subjects. A monoexponential curve fit to the data is shown. To calculate biological half-life and total cumulative urine activity, we fit a curve to the data for each individual subject.

3.3. Radiation-absorbed dose estimates

The average residence time for each source organ, calculated from whole-body images with attenuation correction, is shown in Table 2. Radiation-absorbed dose estimates were calculated and averaged for each subject using the residence times from Table 2 (Table 3). High absorbed doses (in microgray per megabecquerel) were noted for the urinary bladder wall (100), gallbladder wall (83.6), upper large intestine (67.3), lower large intestine (60.6) and small intestine (40.9) at a urine-voiding interval of 4.8 h. Moderate levels of absorbed doses (in microgray per megabecquerel) were seen in the thyroid (39.2), lung (29.1), kidneys (27.6) and liver (18.8) at the same urine-voiding interval. The mean EDE at 2.4- and 4.8-h urine-voiding intervals were estimated to be 3.02×10^{-2} and 3.37×10^{-2} mSv/MBq, respectively.

Table 2
Residence time of each source organ calculated from whole-body images

Organ	Residence time (mean±S.D.)
Brain	0.34±0.09
Thyroid	0.03±0.02
Heart	0.12±0.01
Gallbladder wall	0.30±0.14
Kidneys	0.22±0.08
Lower large intestine	0.57±0.33
Upper large intestine	0.92±0.19
Small intestine	0.89±0.04
Liver	0.61±0.08
Lungs	0.99±0.04
Urinary bladder contents	0.59±0.08[a]
	1.24±0.17[b]
Remainder	6.62±0.37

[a] The residence time of urinary bladder contents was calculated using a dynamic bladder mode implemented in MIRDOSE 3.0 with urine-voiding intervals of 2.4 h.

[b] The residence time of urinary bladder contents was calculated using a dynamic bladder mode implemented in MIRDOSE 3.0 with urine-voiding intervals of 4.8 h.

Table 3
[^{123}I]ADAM radiation doses for adult male (mean±S.D., in microgray per megabecquerel)

Organ	Urine-voiding interval (mean±S.D.)	
	2.4 h	4.8 h
Adrenals	$1.08\times10^{-2}\pm8.54\times10^{-4}$	$1.08\times10^{-2}\pm8.33\times10^{-4}$
Brain	$1.08\times10^{-2}\pm2.32\times10^{-3}$	$1.08\times10^{-2}\pm2.32\times10^{-3}$
Breasts	$5.82\times10^{-3}\pm2.72\times10^{-4}$	$5.83\times10^{-3}\pm2.70\times10^{-4}$
Gallbladder wall	$8.35\times10^{-2}\pm3.42\times10^{-2}$	$8.36\times10^{-2}\pm3.41\times10^{-2}$
LLI wall	$5.88\times10^{-2}\pm2.76\times10^{-2}$	$6.06\times10^{-2}\pm2.74\times10^{-2}$
Small intestine	$4.03\times10^{-2}\pm3.67\times10^{-3}$	$4.09\times10^{-2}\pm3.57\times10^{-3}$
Stomach	$1.08\times10^{-2}\pm8.33\times10^{-4}$	$1.08\times10^{-2}\pm7.77\times10^{-4}$
ULI wall	$6.68\times10^{-2}\pm1.15\times10^{-2}$	$6.73\times10^{-2}\pm1.14\times10^{-2}$
Heart wall	$1.21\times10^{-2}\pm1.53\times10^{-4}$	$1.21\times10^{-2}\pm1.53\times10^{-4}$
Kidneys	$2.75\times10^{-2}\pm7.97\times10^{-3}$	$2.76\times10^{-2}\pm7.97\times10^{-3}$
Liver	$1.88\times10^{-2}\pm2.36\times10^{-3}$	$1.88\times10^{-2}\pm2.35\times10^{-3}$
Lungs	$2.91\times10^{-2}\pm1.22\times10^{-3}$	$2.91\times10^{-2}\pm1.22\times10^{-3}$
Muscle	$8.15\times10^{-3}\pm4.79\times10^{-4}$	$8.58\times10^{-3}\pm4.22\times10^{-4}$
Ovaries	$2.08\times10^{-2}\pm3.12\times10^{-3}$	$2.23\times10^{-2}\pm2.94\times10^{-3}$
Pancreas	$1.22\times10^{-2}\pm1.10\times10^{-3}$	$1.22\times10^{-2}\pm1.05\times10^{-3}$
Red marrow	$8.53\times10^{-3}\pm6.43\times10^{-4}$	$8.76\times10^{-3}\pm6.07\times10^{-4}$
Bone surfaces	$1.37\times10^{-2}\pm8.08\times10^{-4}$	$1.40\times10^{-2}\pm7.55\times10^{-4}$
Skin	$4.82\times10^{-3}\pm2.48\times10^{-4}$	$4.94\times10^{-3}\pm2.31\times10^{-4}$
Spleen	$2.61\times10^{-2}\pm3.70\times10^{-3}$	$2.61\times10^{-2}\pm3.74\times10^{-3}$
Testes	$6.91\times10^{-3}\pm2.46\times10^{-4}$	$8.02\times10^{-3}\pm1.60\times10^{-4}$
Thymus	$7.69\times10^{-3}\pm3.21\times10^{-4}$	$7.69\times10^{-3}\pm3.21\times10^{-4}$
Thyroid	$3.92\times10^{-2}\pm2.47\times10^{-2}$	$3.92\times10^{-2}\pm2.47\times10^{-2}$
Urine bladder wall	$5.14\times10^{-2}\pm5.56\times10^{-3}$	$1.00\times10^{-1}\pm1.25\times10^{-2}$
Uterus	$1.75\times10^{-2}\pm7.64\times10^{-4}$	$2.16\times10^{-2}\pm3.46\times10^{-4}$
Total body	$9.83\times10^{-3}\pm6.78\times10^{-4}$	$1.02\times10^{-2}\pm6.05\times10^{-4}$
EDE[a]	$3.02\times10^{-2}\pm5.11\times10^{-3}$	$3.37\times10^{-2}\pm4.60\times10^{-3}$
ED[a]	$2.60\times10^{-2}\pm4.04\times10^{-3}$	$2.88\times10^{-2}\pm3.96\times10^{-3}$

[a] Units for EDE and ED are millisievert per megabecquerel.

4. Discussion

Our results demonstrate that [^{123}I]ADAM is a pharmacologically safe radioligand, producing neither subjective nor objective side-effects. This finding was also confirmed by clinical physical examinations, serum electrolyte analysis, liver function tests, thyroid function tests and hematological studies before and after administration of the radiotracer. After injection of [^{123}I]ADAM, a majority of the radioactivity (50.32 %ID) was excreted in the urine. This coincided with the urinary bladder wall exhibiting the highest organ absorbed dose of 100 μGy/MBq at a 4.8-h urine-voiding interval, which is still an acceptable dose for routine nuclear medicine practice. Favorable biodistribution of [^{123}I]ADAM in human volunteers was observed, the resulting brain distribution corresponding to 5.02 %ID. The brain SPECT images demonstrated the highest uptake values to be in the brain stem, hypothalamus and pons, which are findings consistent with the known distribution of SERT in the human brain [24]. A relatively steady brain stem SB attained between 3 and 6 h postinjection makes

[^{123}I]ADAM a suitable radiotracer for studying SERT distribution in the brain.

Analysis of the brain SPECT images revealed high uptake of the radiotracer in the hypothalamus, brain stem and pons. Moderate radiotracer uptake was found in the striatum and medial temporal lobe. The above findings confirm observations from in vitro and autoradiographic studies [24], suggesting that [^{123}I]ADAM binds to SERT with a high affinity and specificity in the living human brain. These observations, taken in conjunction with the fact that [^{123}I]ADAM is not known to cross-bind with other monoamine transporters, make it a superior SPECT radioagent for targeting SERT, as compared to [^{123}I]beta-CIT [15]. However, determining the concentration of SERT in the frontal cortex still presents a challenge. We observed a peak SB value of 0.16 at 135 min postinjection from the dynamic study. Similar observations were noted in our previous study involving the biodistribution of the rat brain: brain regions with a smaller density of SERT reach a transit equilibrium at an early time period [17]. Low uptake and large variation of [^{123}I]ADAM in the frontal cortex can also be seen in the 3- to 5-h postinjection studies. Serotonin transporter evaluation at the frontal cortex remains unsolved using a SPECT radiotracer. An additional limitation is that small brain regions cannot be easily delineated on SPECT images. Radioactivity uptake in the medial temporal lobe seen at 4 h suggests that substantial SERT distribution exists in the hippocampus and amygdala regions. However, the ROI is difficult to identify and the partial volume effect may result in an underestimation of the uptake value. Evaluation of the medial temporal lobe SERT quantity is possible by fusing the functional SPECT image to its corresponding MRI image. The MRI image provides an accurate anatomical reference for the SPECT images.

Single photon emission computed tomography images acquired immediately after tracer injection showed a substantial uptake of the drug in the whole brain including the cortex, striatum, thalamus, hypothalamus, medial temporal lobe, brain stem and cerebellum, suggesting an acceptable level of penetration of the brain–blood barrier. The sequential images showed a rapid clearance of the radiotracer from nonspecific binding sites including the cortex, striatum and cerebellum. The SB in the hypothalamus and brain stem gradually increased over time and reached a peak value of 1.44 at 4 h postinjection. The time period necessary to achieve transit equilibrium was consistent with the recommendations from Newberg et al. [21]. However, our peak SB value was higher than that recorded by Newberg et al. [21]. The reason for this difference is not clear, as a similar analytic method was applied in both studies. Some possible factors affecting the peak SB value include the age group or ethnic origin of the subjects included in the study, the protocol used for drug preparation and the method used to define ROIs and cerebellum boundaries. If the above factors have a significant affect on the final SB value, it may be difficult to compare SB values between different studies. However, further investigation with a larger number of study subjects will be needed before drawing any conclusions.

The distribution of [^{123}I]ADAM binding in the brain was very similar to distributions obtained using other SERT tracers, such as C-11 (+) McN5652 and C-11 DASB; however, the midbrain radiotracer uptake was somewhat different [11,25,26]. The PET tracers C-11 (+) McN5652 and C-11 DASB exhibit an average midbrain to cerebellum ratio of 1.2 ± 0.34 and 2.04 ± 0.44, respectively [26]. The kinetics of [^{123}I]ADAM appears to be much slower than the C-11 tracers, reaching a near steady state 3 h after tracer injection. The relatively constant SB of [^{123}I]ADAM in the brain stem between 3 and 6 h postinjection provides an optimal time window for brain SPECT imaging in routine nuclear medicine practice.

Investigations of the biodistribution of [^{123}I]ADAM have recently been published by Newberg et al. [21] and Kauppinen et al. [22]. Our results using attenuation correction images for dosimetry calculation are similar to those cited by Newberg et al. [21], despite methodological differences. We measured direct urine radioactivity counts for input into the dynamic urinary model, whereas Newberg et al. [21] determined urine radioactivity counts from the whole-body image. Because the majority of the injected dose was excreted in the urine, the amount of radioactivity in the urine must be carefully measured for an accurate quantification of the radiation dose. To minimize errors in radioactivity measurement, the volume of urine used for radioactivity measurement corresponded to the volume used for calibration of the well gamma counter. Because the injected drugs were also measured in a similar geometry, this measurement of urine radioactivity may be more accurate than that from whole-body images. This may account for differences in the radiation dose estimation from the urinary bladder wall in our result as compared with others. The sum of the urine %ID measured by direct counting and the whole-body %ID measured from images at 6 h postinjection (before defecation) was 98.9 ± 1.4%, indicating acceptable recovery of urine and an integration of these two methods. The radiation-absorbed dose in the urinary bladder wall and the total body EDE can undergo a 49% and 10% reduction, respectively, by shortening the urine-voiding intervals from 4.8 to 2.4 h; therefore, individuals should be encouraged to empty their bladders frequently in order to decrease the radiation burden. To prevent the underestimation of radiation-absorbed doses, we performed analyses using conservative procedures. These analyses included placement of large ROIs on source organs and assuming physical decay only after the last whole-body imaging at 24 h postinjection.

Attenuation of radioactivity by tissues can also affect the measurement of radioactivity [27]. For example, the lungs attenuate the least amount of activity because they are filled with air, whereas solid organs such as the liver will attenuate the greatest amount of radioactivity. In this study, for example, the liver demonstrated a high initial uptake of the

injected radiotracer. The largest increase in %ID was found in the gallbladder (51%), followed by the bladder (46%), kidney (43%), intestine (41%) and liver (40%) after attenuation correction. Minute changes in %ID were noted in the lung (−2%). The %ID of the remainder of the body was overestimated by 15% before attenuation correction. Although the radiotracer used for attenuation in the present study was different from those used by Newberg et al. [21] (i.e., ^{99m}Tc vs. ^{123}I), the resulting estimates of the attenuation coefficients were similar. These data are further supported by data from Newberg et al. [21] indicating that attenuation correction has a significant impact on the evaluation of dosimetry.

A surge of radioactivity in the brain and the remainder of the body was seen 40 min after radiotracer injection in both the whole-body and dynamic brain SPECT images. This surge in radioactivity was found in both SERT-rich and nonrich sites in the brain. The radioactivity surge observed in the brain and blood was countered by a simultaneous decrease in radioactivity in the lungs, leading to the speculation that the phenomenon was caused by a redistribution of the radiotracer. As suggested by Suhara et al. [28], the lungs may function as a reservoir for drugs that target the SERT. Excretion of the radiotracer from the lungs could lead to increased concentrations of radioactivity in the blood, thus, increasing the radioactivity in the brain. As demonstrated by the whole-body distribution results, the amount of brain SERT was relatively small compared with that in the lungs. The pharmacokinetics and drug interaction between central and peripheral SERTs must be carefully investigated in order to accurately estimate SERT function in the brain.

5. Conclusion

The postinjection kinetics of [^{123}I]ADAM were favorable, showing a gradual increase in [^{123}I]ADAM SB in the brain stem at 3 h, achieving a maximum of 1.44 at approximately 4 h, and remaining constant until 6 h. During this time period, a high uptake of ADAM can be identified in known SERT-rich sites, including the hypothalamus, brain stem, pons and medial temporal lobe. The [^{123}I]ADAM EDE for an adult male, calculated using attenuation-corrected images, was 3.37×10^{-2} mSv/MBq. Based on the average EDE value derived from this study, subjects would receive an EDE of approximately 6.23 mSv using a general injection dose of 185 MBq [^{123}I]ADAM, which is comparable to the average EDE per patient in other ^{123}I studies using standard nuclear medicine procedures [29–32]. However, redistribution of the tracer from extracerebral compartments (such as the lung) to plasma and brain must be carefully taken into consideration while quantifying the SB in the brain. Taken in conjunction with results from previous studies [21,22], our data suggest that [^{123}I]ADAM is a promising SPECT radiotracer for the study of SERT in the human brain.

Acknowledgments

The authors thank Anita Dhyani for her useful comments on this manuscript. This project was supported by the National Science Council-Taiwan (NSC 92-NU-7-182A-002 and NSC 93-2314-B-182A-076) and Chang Gung Memorial Hospital (CGMPG 340006 and CGRPG 34007).

References

[1] Tejanibutt SM, Yang JX, Pawlyk AC. Altered serotonin transporter sites in Alzheimer's disease raphe and hippocampus. Neuroreport 1995;6:1207–10.
[2] Malhotra AK, Goldman D, Mazzanti C, Clifton A, Breier A, Pickar D. A functional serotonin transporter (5-HTT) polymorphism is associated with psychosis in neuroleptic-free schizophrenics. Mol Psychiatry 1998;3:328–32.
[3] Kuikka J, Tammela L, Rissanen A, Bergstrom K, Muhonen M, Vanninen E, et al. Altered serotonin transporter density in obese binge eating women: initial findings. Eur J Nucl Med Mol Imaging 2000; 27:S90.
[4] Stengler-Wenzke K, Muller U, Angermeyer MC, Sabri O, Hesse S. Reduced serotonin transporter-availability in obsessive–compulsive disorder (OCD). Eur Arch Psychiatry Clin Neurosci 2004;254:252–5.
[5] Ogilvie AD, Battersby S, Bubb VJ, Fink G, Harmar AJ, Goodwin GM, et al. Polymorphism in serotonin transporter gene associated with susceptibility to major depression. Lancet 1996;347:731–3.
[6] Owens MJ, Nemeroff CB. Role of serotonin in the pathophysiology of depression — focus on the serotonin transporter. Clin Chem 1994; 40:288–95.
[7] Wolf WA, Kuhn DM. Modulation of serotonin release. Interactions between the serotonin transporter and autoreceptors. Ann N Y Acad Sci 1990;604:505–13.
[8] Arango V, Underwood MD, Mann JJ. Serotonin brain circuits involved in major depression and suicide. Prog Brain Res 2002; 136:443–53.
[9] Arango V, Underwood MD, Mann JJ. Postmortem findings in suicide victims — implications for in vivo imaging studies. Ann N Y Acad Sci 1997;836:269–87.
[10] Hiltunen J, Akerman KK, Kuikka JT, Bergstrom KA, Halldin C, Nikula T, et al. Iodine-123 labeled nor-beta-CIT as a potential tracer for serotonin transporter imaging in the human brain with single-photon emission tomography. Eur J Nucl Med Mol Imaging 1998;25: 19–23.
[11] Houle S, Ginovart N, Hussey D, Meyer JH, Wilson AA. Imaging the serotonin transporter with positron emission tomography: initial human studies with [C-11]DAPP and [C-11]DASB. Eur J Nucl Med Mol Imaging 2000;27:1719–22.
[12] Baldwin RM, Zeaponce Y, Zoghbi SS, Laurelle M, Altikriti MS, Sybirska EH, et al. Evaluation of the monoamine uptake site ligand [I-123] methyl 3-beta-(4-iodophenyl)-tropane-2-beta-carboxylate ([I-123]beta-CIT) in nonhuman-primates — pharmacokinetics, biodistribution and SPECT brain imaging coregistered with MRI. Nucl Med Biol 1993;20:597–606.
[13] Scheffel U, Dannals RF, Cline EJ, Ricaurte GA, Carroll FI, Abraham P, et al. [I-123-125I]RTI-55, an in vivo label for the serotonin transporter. Synapse 1992;11:134–9.
[14] Brucke T, Kornhuber J, Angelberger P, Asenbaum S, Frassine H, Podreka I. SPECT imaging of dopamine and serotonin transporters with [123I]beta-CIT. Binding kinetics in the human brain. J Neural Transm Gen Sect 1993;94(2):137–46.
[15] Fujita M, Takatoku K, Matoba Y, Nishiura M, Kobayashi K, Inoue O, et al. Differential kinetics of [I-123]beta-CIT binding to dopamine and serotonin transporters. Eur J Nucl Med Mol Imaging 1996;23: 431–6.

[16] Lin KJ, Ye XX, Yen TC, Wey SP, Tzen KY, Ting G, et al. Biodistribution study of [(123)I] ADAM in mice: correlation with whole body autoradiography. Nucl Med Biol 2002;29:643–50.
[17] Lin KJ, Yen TC, Wey SP, Hwang JJ, Ye XX, Tzen KY, et al. Characterization of the binding sites for I-123-ADAM and the relationship to the serotonin transporter in rat and mouse brains using quantitative autoradiography. J Nucl Med 2004;45:673–81.
[18] Oya S, Choi SR, Hou C, Mu M, Kung MP, Acton PD, et al. 2-(2-((Dimethylamino)methyl)phenyl)thio-5-iodophenylamine (ADAM): an improved serotonin transporter ligand. Nucl Med Biol 2000;27:249–54.
[19] Huang WS, Ma KH, Cheng CY, Chen CY, Fu YK, Chou YH, et al. Imaging serotonin transporters with [^{123}I]ADAM brain SPECT in healthy non-human primates. Nucl Med Commun 2004;25:515–9.
[20] Acton PD, Choi SR, Hou C, Plossl K, Kung HF. Quantification of serotonin transporters in nonhuman primates using [(123)I]ADAM and SPECT. J Nucl Med 2001;42:1556–62.
[21] Newberg AB, Plossl K, Mozley PD, Stubbs JB, Wintering N, Udeshi M, et al. Biodistribution and imaging with I-123-ADAM: a serotonin transporter imaging agent. J Nucl Med 2004;45:834–41.
[22] Kauppinen TA, Bergstrom KA, Heikman P, Hiltunen J, Ahonen AK. Biodistribution and radiation dosimetry of [I-123]ADAM in healthy human subjects: preliminary results. Eur J Nucl Med Mol Imaging 2003;30:132–6.
[23] Kish SJ, Furukawa Y, Chang LJ, Tong JC, Ginovart N, Wilson A, et al. Regional distribution of serotonin transporter protein in postmortem human brain — is the cerebellum a SERT-free brain region? Nucl Med Biol 2005;32:123–8.
[24] Varnas K, Halldin C, Hall H. Autoradiographic distribution of serotonin transporters and receptor subtypes in human brain. Hum Brain Mapp 2004;22:246–60.
[25] Szabo Z, Kao PF, Scheffel U, Suehiro M, Mathews WB, Ravert HT, et al. Positron emission tomography imaging of serotonin transporters in the human brain using [11C](+)McN5652. Synapse 1995;20:37–43.
[26] Szabo Z, Scheffel U, Mathews WB, Ravert HT, Szabo K, Kraut M, et al. Kinetic analysis of [C-11]McN5652: a serotonin transporter radioligand. J Cereb Blood Flow Metab 1999;19:967–81.
[27] Ferrant A, Cauwe F. Quantitative organ-uptake measurement with a gamma camera. Eur J Nucl Med 1979;4:223–9.
[28] Suhara T, Sudo Y, Yoshida K, Okubo Y, Fukuda H, Obata T, et al. Lung as reservoir for antidepressants in pharmacokinetic drug interactions. Lancet 1998;351:332–5.
[29] Ueda M, Iida Y, Mukai T, Mamede M, Ishizu K, Ogawa M, et al. 5-[123I]Iodo-A-85380: assessment of pharmacological safety, radiation dosimetry and SPECT imaging of brain nicotinic receptors in healthy human subjects. Ann Nucl Med 2004;18:337–44.
[30] Lahorte CM, Bacher K, Burvenich I, Coene ED, Cuvelier C, De PC, et al. Radiolabeling, biodistribution, and dosimetry of (123)I-mAb 14C5: a new mAb for radioimmunodetection of tumor growth and metastasis in vivo. J Nucl Med 2004;45:1065–73.
[31] Fujita M, Seibyl JP, Vaupel DB, Tamagnan G, Early M, Zoghbi SS, et al. Whole-body biodistribution, radiation absorbed dose, and brain SPET imaging with [123i]5-i-A-85380 in healthy human subjects. Eur J Nucl Med Mol Imaging 2002;29:183–90.
[32] Schmidt D, Langen KJ, Herzog H, Wirths J, Holschbach M, Kiwit JC, et al. Whole-body kinetics and dosimetry of L-3-^{123}I-iodo-alpha-methyltyrosine. Eur J Nucl Med 1997;24:1162–6.